X-Ray Standing Waves at a Reflecting Mirror Surface

M. J. Bedzyk,[1] G. M. Bommarito,[2], and J. S. Schildkraut[3]
[1]*Cornell High Energy Synchrotron Source and The School of Applied and Engineering Physics, Cornell University, Ithaca, New York, 14853*
[2]*Department of Chemistry, Cornell University, Ithaca, New York 14853*
[3]*Corporate Research Laboratories, Eastman Kodak Company, Rochester, New York 14650*
(Received 11 January 1989)

X-ray standing waves generated above a gold mirror surface during total external reflection are used to locate unambiguously a zinc-ion layer which is embedded ≈ 200 Å above the mirror surface in a Langmuir-Blodgett multilayer with a precision of 2 Å.

PACS numbers: 61.10.−i, 07.85.+n, 61.30.−v, 68.35.Bs

The conventional method for generating x-ray standing waves (XSW) has been to use dynamical Bragg diffraction from perfect single crystals. As first demonstrated by Batterman,[1] the standing wave inside the crystal has a period equal to the diffraction-plane spacing and a phase that depends on the incident angle θ. After Andersen, Golovchenko, and Mair[2] pointed out that x-ray standing waves extend above the crystal surface, this interference effect was used by Cowan, Golovchenko, and Robbins[3] to locate the position of an adsorbate atom layer on a perfect single-crystal surface. This positional information is obtained by observing the modulation in the adsorbate-atom fluorescence as the standing-wave antinodes shift inward by one-half of a d spacing during a scan in angle θ through the Bragg reflection. With a period ranging from 1 to 4 Å, this conventional XSW technique has proven to be very precise in determining the bond-length distances that separate adsorbate atoms from the surface-bulk-lattice positions.[3,4] However, since the period is fixed to the d spacing, these measurements have an inherent modulo-d ambiguity in the determined position.

In this Letter, we will describe how an x-ray standing wave with a variable period, ranging from 70 to 1000 Å, can be generated by the total external reflection of a monochromatic x-ray beam from a mirror surface. Furthermore, we will demonstrate how this new x-ray probe can be used to precisely and unambiguously locate a layer of heavy atoms embedded in a low-Z thin film, which is deposited on the mirror surface.

Whenever an electromagnetic traveling wave impinges on a boundary separating two materials of different indices of refraction, part of the wave energy is reflected and the remainder is transmitted (or refracted). Since the index of refraction n for x rays in matter is less than unity, x rays undergo total external reflection when θ is less than the critical angle θ_c. [For $n=1-\delta-i\beta$, where δ and β are $\leq 10^{-5}$, $\theta_c=(2\delta)^{1/2}$.]

Referring to Fig. 1, if we take the incident and reflected wave vectors, $\mathbf{k}_0$ and $\mathbf{k}_R$, to lie in the x-z plane with the z axis pointing along the surface normal direction, and apply the necessary boundary conditions, the incident and reflected traveling E-field plane waves can be described as

$$\bar{\epsilon}_0(\mathbf{r},t)=\mathbf{E}_0\exp\{i[\omega t-2\pi(k_x x-k_z z)]\}\,,$$

$$\bar{\epsilon}_R(\mathbf{r},t)=\mathbf{E}_R\exp\{i[\omega t-2\pi(k_x x+k_z z)]\}\,.$$

For convenience, the surface will be at $z=0$, and for our discussion, we will only consider the case of σ polarization (i.e., $\mathbf{E}_0$ and $\mathbf{E}_R$ will be perpendicular to the x-z plane).

By locating the intersections of the crests and troughs of the two plane waves in Fig. 1, one can easily show that the interference between the two coherent traveling plane waves generates a standing wave with planes of maximum intensity parallel to the surface and with a period $D=\lambda/2\sin\theta$. This describes the distance between the first antinode and successive antinodes of the standing wave. To find the distance between the first antinode and the surface, we only need to describe the relative phase v between the reflected and incident E-field amplitudes. This can be accomplished by using the Fresnel coefficient for reflection[5,6] which describes the complex-wave-amplitude ratio[7] for the vacuum/solid interface as

$$\frac{E_R}{E_0}=\frac{|E_R|}{|E_0|}e^{iv}=\frac{\theta-(\theta^2-2\delta-2i\beta)^{1/2}}{\theta+(\theta^2-2\delta-2i\beta)^{1/2}}\,.$$

Universal curves describing the phase v and the reflectivity $R=|E_R/E_0|^2$ are plotted in Fig. 2(a) as functions of normalized angle $x=\theta/\theta_c$ for the case of $\beta=0$

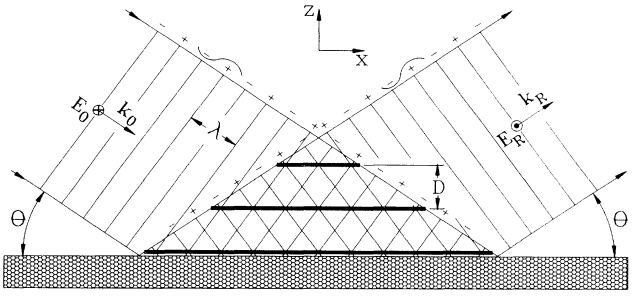

FIG. 1. Illustration of the x-ray standing-wave field formed by the interference between the incident and specular-reflected plane waves above a mirror surface.

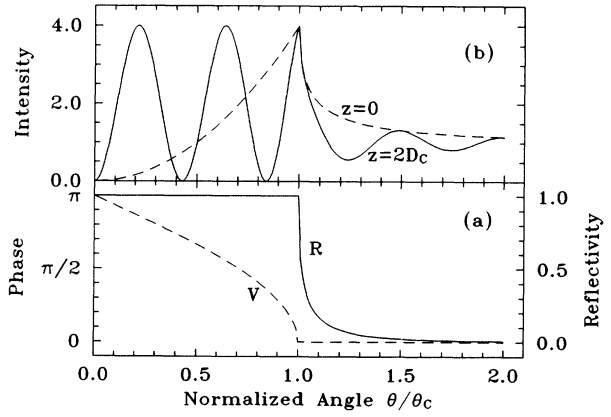

FIG. 2. For $\beta=0$. (a) The angular dependence of the reflectivity R and relative phase v of the reflected plane wave. (b) The angular dependence of the E-field intensity at $z=0$ and $z=2D_c$ for $|E_0|=1$.

(i.e., no absorption). For $\beta=0$, the phase, which can be expressed as $v=\cos^{-1}(2x^2-1)$, decreases from π to 0 as θ is increased from 0 to θ_c. The reflectivity remains at $R=1$ over this same angle range for $\beta=0$. Therefore, as θ increases from 0 to θ_c, the E-field intensity $|\bar{\epsilon}_0+\bar{\epsilon}_R|^2$ at the surface changes smoothly from 0 to $4|E_0|^2$, or from a node to an antinode. Since the period $D=\lambda/2\sin\theta$, the first antinode is at infinity for $\theta=0$. As θ is increased from 0 to θ_c, the first antinode moves inward until it coincides with the mirror surface at $\theta=\theta_c$. Because of the decrease in period D, the remaining antinodes move inward like a compressing bellows as θ is increased. The compression of the standing wave, which is due to the period decreasing, and the shifting inward of the standing wave, which is due to the phase decreasing, are expressed in terms of the E-field intensity in the vacuum above the surface as

$$I(\theta,z)=|E_0|^2[1+R+2\sqrt{R}\cos(v-2\pi Qz)],$$

where $Q=2\sin\theta/\lambda=1/D$ is the magnitude of the wave-vector transfer $\mathbf{Q}=\mathbf{k}_R-\mathbf{k}_0$. The angle θ dependence of the E-field intensity I is plotted in Fig. 2(b) for $z=0$ and $z=2D_c$, where the critical period D_c is the standing-wave period at $\theta=\theta_c$. The critical period is

$$D_c=\lambda/2\theta_c=(\sqrt{\pi}/2)[N_a r_e(Z+f')]^{-1/2},$$

where N_a is the atom density, r_e is the classical electron radius, Z is the atomic number, and f' is the anomalous-dispersion correction. Ignoring anomalous-dispersion effects, D_c is an energy-independent parameter, which is 77 Å for a gold mirror and 200 Å for a silicon mirror.

Since the photoelectric-effect cross section is proportional to the E-field intensity at the center of an atom (in the dipole approximation), we can observe the angle θ dependence of the standing wave, as shown in Fig. 2(b), by monitoring the fluorescence signal from a marker layer of atoms that is a mean distance $\langle z\rangle$ above the mirror surface. Observing the π radian phase shift can most easily be done by placing the marker layer at the surface. This is the well-known evanescent-wave condition,[8] which has the surface intensity going from a node to an antinode as θ increases from 0 to θ_c. This effect, which is described by the $z=0$ curve in Fig. 2(b), is routinely used for enhancing surface fluorescence and surface diffraction. To clearly observe the compression of the standing wave as θ increases, the following conditions should be created experimentally: (1) the mean position of the marker layer $\langle z\rangle$ should be greater than the critical period D_c, (2) the marker layer width $\langle z^2\rangle^{1/2}$ should be much smaller than $\langle z\rangle$, and (3) the refractive effects of the overlayer that contains the marker layer should be much weaker than the refractive effects of the mirror.

In an earlier study,[9] we used standing waves generated by Bragg diffraction to locate a layer of zinc ions that was suspended in a Langmuir-Blodgett (LB) trilayer at $\langle z\rangle=53$ Å above a silicon-tungsten-layered synthetic microstructure. We also looked at this Zn layer with standing waves generated by total external reflection. However, since this 53-Å distance was much smaller than the effective SiW critical period, we could only observe the first antinode passing through the Zn layer. To observe the full effect, we chose in the present study to use a gold mirror, coated with a $\approx$250-Å thick hydrocarbon film made of several LB bilayers in which a layer of zinc ions is contained in the topmost LB bilayer. The Zn distance, in this case, is roughly 3 times the critical period, and therefore three antinodes pass through the Zn layer as the angle θ is increased from 0 to θ_c. The corresponding observed Zn $K\alpha$ fluorescence modulations are shown in Fig. 3(b) along with the simultaneously collected reflectivity shown in Fig. 3(a).

A schematic cross-sectional view of the sample is shown in the inset of Fig. 3(b). The 25-mm-wide by 50-mm-long gold mirror consisted of 250 Å of gold evaporated onto a chromium-coated float glass. After plasma cleaning the gold surface, a 25-Å thick monolayer of octadecyl thiol (ODT) was absorbed onto the gold to form a uniformly thick hydrophobic surface for the subsequent LB deposition of a 56-Å thick cadmium arachadate (CdA) bilayer, followed by the deposition of two 60-Å thick ω-tricosanoic acid (ωTA) LB bilayers, followed by the deposition of a 55-Å thick zinc arachadate (ZnA) bilayer. The LB multilayer covered the entire mirror surface except for a 15-mm length at one end. The above-quoted thicknesses for the layers assume that the hydrocarbon chains in each layer are fully extended and perpendicular to the mirror surface. Using the optical constants of the mirror and assuming the film to be isotropic with an index of refraction of 1.55 at 632 nm, the thickness of the multilayer over its entire area was measured by ellipsometry to be 215 Å. This is 41 Å less than that predicted by the fully extended untilted hydro-

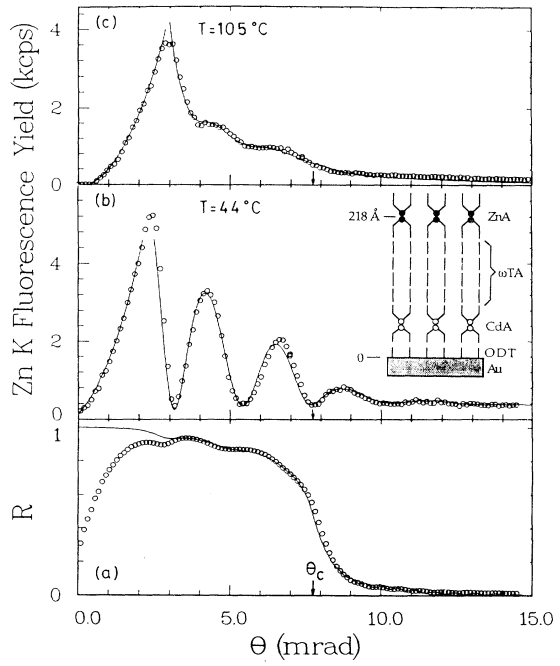

FIG. 3. (a) The angular dependence of the reflectivity at 9.8 keV for the LB film/Au mirror schematically depicted in the inset. (b) The angular dependence of the Zn $K\alpha$ fluorescence count rate at $T=44\,^{\circ}\mathrm{C}$, and (c) at $T=105\,^{\circ}\mathrm{C}$. The circles are experimental and the solid lines are theoretical. Inset: Circles represent heavy atoms and line segments represent hydrocarbon chains.

carbon-chain approximation.

The experiment was carried out at the Cornell High Energy Synchrotron Source (CHESS). The bending-magnet radiation from the Cornell Electron Storage Ring (CESR) was monochromated by a pair of Ge(111) crystals to an x-ray energy of $E_\gamma=9.8$ keV for optimally exciting Zn K fluorescence. Both the monochromator and the Au mirror sample were set up to reflect the vertical plane. The 25-mm-wide by 35-mm-long sample surface was exposed to an incident beam that had a width of 2 mm and a height of 0.07 mm. This beam height subtends the entire 35-mm sample length at $\theta=2$ mrad. [This geometrical effect is responsible for the drop in reflectivity below 2 mrad in Fig. 3(a).] An energy-dispersive solid-state detector was positioned perpendicular to the incident beam to collect the fluorescence at a glancing angle with respect to the surface. The sample was maintained in a helium-filled oven with a temperature stability of $\pm 1\,^{\circ}\mathrm{C}$. The first data set was taken at $T=44\,^{\circ}\mathrm{C}$. The measured reflectivity and Zn $K\alpha$ fluorescence yield for this scan in θ are shown in Figs. 3(a) and 3(b). Subsequent scans were taken at $10\,^{\circ}\mathrm{C}$ increments from $50\,^{\circ}\mathrm{C}$ to $90\,^{\circ}\mathrm{C}$, and then in $5\,^{\circ}\mathrm{C}$ intervals from $90\,^{\circ}\mathrm{C}$ to $130\,^{\circ}\mathrm{C}$. Similar to our earlier finding[9] for a ZnA bilayer on a CdA monolayer, a strong irreversible transition was observed at $T=100\,^{\circ}\mathrm{C}$. The scan for $T=105\,^{\circ}\mathrm{C}$ is shown in Fig. 3(c). Each scan took ≈ 15 min. The sample was allowed to equilibrate at the new temperature for ≈ 20 min before each subsequent scan.

The data taken before reaching $95\,^{\circ}\mathrm{C}$ did not differ significantly from the initial $T=44\,^{\circ}\mathrm{C}$ scan shown in Figs. 3(a) and 3(b). The data taken after passing $100\,^{\circ}\mathrm{C}$ and then returning to room temperature differed only slightly from the $T=105\,^{\circ}\mathrm{C}$ scan shown in Fig. 3(c). The $T=95\,^{\circ}\mathrm{C}$ scan was halfway between the pre- and post-transition form.

In Fig. 3(b), there are three complete modulations in the Zn $K\alpha$ fluorescence, between $\theta=0$ and $\theta=\theta_c$. Comparing this to the E-field intensity modulations in Fig. 2(b) qualitatively indicates that the Zn layer is at $\langle z\rangle \simeq 2.5D_c=200$ Å. Comparing the amplitudes of the modulations in Figs. 3(b) and 3(c) indicates that the Zn layer thickness is small before the transition and large afterwards. The modulations for the $T=105\,^{\circ}\mathrm{C}$ Zn fluorescence become weaker as θ increases, due to the standing-wave period becoming smaller than the Zn layer thickness at higher θ.

In order to more precisely quantify the mean position $\langle z\rangle$ and width $\langle z^2\rangle^{1/2}$ of the Zn layer, we have χ^2 fitted our data to theoretical yields based on a layered model. The starting model has a layered arrangement as depicted in the inset for Fig. 3(b). Each layer is characterized in the calculation by a thickness and index of refraction. The total E field at any position z in a layer can be calculated by using Parratt's recursion formulation[6] for determining the E-field amplitudes at the boundaries surrounding the layer. From this we can calculate the E-field intensity at any Zn position z in the model. For simplicity, we assume that the Zn is in a Gaussian distribution.

Parratt's recursion formulation directly gives the reflectivity from this layered model. This is shown in Fig. 3(a). The two small steps in the reflection curve at 2.5 and 4.5 mrad correspond to the critical angles for the thin Zn and Cd layers, respectively. The critical angle for these layers is smaller than θ_c for Au, due to lower electron densities.

Based on the theoretical fit[10] to the $T=44\,^{\circ}\mathrm{C}$ Zn fluorescence data in Fig. 3(b), the Zn layer is at a mean position of $\langle z\rangle=218$ Å above the Au surface and has a width of $2\sigma=24$ Å. Both $\langle z\rangle$ and 2σ were determined with a precision of 2 Å. The 218-Å value is only 11 Å shorter than the expected length for fully extended and untilted hydrocarbon chains. The 24-Å width is primarily a measure of the rms surface roughness of the gold mirror.

For the fit to the $T=105\,^{\circ}\mathrm{C}$ data in Fig. 3(c), $\langle z\rangle=174$ Å and $2\sigma=110$ Å. The underlying structural change in the film that leads to this inward spread of the Zn layer cannot be completely determined from this result, since this measurement is only directly sensitive (via fluorescence) to the heavy-atom distributions in the film. To this end, we are studying this thermotropic transition with depth-selective in-plane x-ray diffraction.[11]

As a corollary, we note that since this new type of x-ray standing wave has a variable period, it can be used to describe the heavy-atom distribution $\rho(z)$ in the low-Z film above the mirror with more detail than just giving the two parameters $\langle z\rangle$ and $\langle z^2\rangle^{1/2}$. It can in fact be used to discriminate between different types of distributions (e.g., rectangular or Gaussian), which have the same $\langle z\rangle$ and $\langle z^2\rangle^{1/2}$. In effect, we can determine the Fourier transform of $\rho(z)$ over a continuous range in Q from 0 to $1/D_c$. Therefore, total-external-reflection standing-wave data can lead directly to a determination of $\rho(z)$ at a 2-Å level of resolution. In contrast to this, a Bragg-diffraction-generated standing wave has essentially a fixed period d and can therefore only be used to determine one discrete Fourier-type component of $\rho(z)$ corresponding to $Q=H=1/d$.

In conclusion, we have demonstrated how x-ray standing waves can be generated above a mirror surface during total external reflection. Furthermore, we have shown how this new application of x-ray standing waves can be used to unambiguously locate heavy atoms at length scales of hundreds of angstroms above a mirror surface with angstrom-level precision.

The authors are grateful for the contributions made by M. Caffrey, D. H. Bilderback, N. Tillman, and B. W. Batterman. This work was supported by CHESS under NSF Grant No. DMR-87-19764.

[1]B. W. Batterman, Phys. Rev. **133**, A759 (1964); Phys. Rev. Lett. **22**, 703 (1969).

[2]S. K. Andersen, J. A. Golovchenko, and G. Mair, Phys. Rev. Lett. **37**, 1141 (1976).

[3]P. L. Cowan, J. A. Golovchenko, and M. F. Robbins, Phys. Rev. Lett. **44**, 1680 (1980).

[4]J. A. Golovchenko, J. R. Patel, D. R. Kaplan, P. L. Cowan, and M. J. Bedzyk, Phys. Rev. Lett. **49**, 560 (1982); M. J. Bedzyk and G. Materlik, Phys. Rev. B **31**, 4110 (1985).

[5]A. H. Compton and S. K. Allison, *X-Rays in Theory and Experiment* (Van Nostrand, New York, 1935).

[6]L. G. Parratt, Phys. Rev. **95**, 359 (1954).

[7]An equivalent expression for E_R/E_0 can be derived from dynamical diffraction theory [see B. W. Batterman and H. Cole, Rev. Mod. Phys. **36**, 681 (1961)] by solving for the symmetric zeroth-order Bragg diffraction condition. (For example, set the structure factor $F_H=F_0$ in the expression for angle parameter η.) This agreement between the optical theory and dynamical diffraction theory simply means that the total external reflection of x rays from a sharp interface is equivalent to Bragg diffraction from a set of crystal planes with an infinite d spacing.

[8]W. C. Marra, P. Eisenberger, and A. Y. Chou, J. Appl. Phys. **50**, 6927 (1979); R. S. Becker, J. A. Golovchenko, and J. R. Patel, Phys. Rev. Lett. **50**, 153 (1983); J. M. Bloch, M. Sansone, F. Rondelez, D. G. Peiffer, P. Pincus, M. W. Kim, and P. M. Eisenberger, Phys. Rev. Lett. **54**, 1039 (1985).

[9]M. J. Bedzyk, D. H. Bilderback, G. M. Bommarito, M. Caffrey, and J. S. Schildkraut, Science **241**, 1788 (1988).

[10]The theoretical curves in Figs. 3(b) and 3(c) were given two geometrical corrections. The first corrected for the finite height of the beams subtending less Zn as θ increased, and the second corrected for the Zn yield increasing as θ increased due to the finite aperture of the solid-state detector.

[11]The depth selectivity is obtained by moving the XSW antinode to a layer of atoms and thereby enhancing the x-ray scattering from that layer.